Design, analysis and model fabrication of vertical axis wind turbine

Certification of Approval

This final year project report under the title of **"Design, analysis and model fabrication of vertical axis wind turbine"** is submitted to the Institute of Mechanical and Manufacturing Engineering (IMME), Khwaja Fareed University of Engineering and Information Technology, Rahim Yar Khan, Pakistan (KFUEIT) in partial fulfillment of the requirements for the degree of **BS Mechanical Engineering**.

Supervisor	Co-supervisor
Engr. Dr. Mumtaz Ahmad Qaisrani Assistant Professor IMME, KFUEIT	Engr. Muhammad Zahid Lecturer IMME, KFUEIT

FYP Examiner	External Examiner

Head of Department

ACKNOWLEDGMENT

In the name of the Most Gracious and Merciful ALLAH. He is the one who gave us the courage to finish this research project. This research Project titled "**Design, analysis and model fabrication of vertical axis wind turbine**" was completed at department of mechanical engineering Khwaja Fareed University of Engineering and Information Technology, Rahim Yar Khan, under the PEC annual Awards of Final Year Design Project (FYDP) for the year 2022-2023. The project was completed under the supervision of Dr. Mumtaz A. Qaisrani.

.

ABSTRACT

The available types of wind turbines will be reviewed in this report. The large-scale production and use of wind energy is being practiced due to the remarkable advances in the science, technology, and design in the current era. Being environmentally friendly, the wind turbines convert and modify the kinetic energy of wind into electrical power. A very definite and promising future is represented by the vertical axis wind power generators for wind power generation. A H-Rotor vertical axis wind turbine is a most suitable turbine for a specific and particular setting and provides a new outlook to the vertical axis wind turbine. From grinding grains to producing electricity, the growth of wind technology is worthwhile. For residential and commercial areas, vertical axis wind turbines are mostly used, while for the wind farms, horizontal axis wind turbines are more preferred in rural areas and offshore. The vertical axis wind turbines offer direct rotary output. They are not required to be oriented in wind direction. In this report, a VAWT three blades are being used. Blades are the main component of our project. The designing of blades is very important and significant. Because the blades are responsible for extracting energy form the air. NACA 0018 profile is used for designing the blades. These blades work on the basis of lift. When the air strikes on the curve sides of the blades, this creates the pressure difference around the blades which rotate due to pressure difference. This is not drag based but lift based. For the rotation of blades, we use 3.88 m/s wind speed. Bearing and gears are also used to get maximum result. This project is basically focused on the design and fabrication of H-rotor vertical axis wind turbine. Application and limitation of this project also has been discussed. Such a project is suitable for areas where average air speed is relatively high. A DC generator is used to produce electricity power for mechanical power. The output at the generator will be available to use for appliances. H-rotor vertical axis wind turbine is easy to design and to fabricate than other types of vertical axis wind turbine.

Dedication

Dedicated to our beloved parents for their prayers and our teachers, for their endless support and guidance that lead us towards that accomplishment.

Table of Contents

List of Figures

List of Tables

NOMENCLATURE

P	Power (W)
S	Thrust (N)
T	Torque (Nm)
C_L	Coefficient of Lift
C_D	Coefficient of Drag
C_P	Coefficient of Performance
C_n	Normal Force Coefficient
C_t	Tangential Force Coefficient
L	Blade Length (m)
A	Swept Area (m^2)
V	Velocity (m/s)
W	Relative Wind Velocity(m/s)
C	Chord Length (m)

Greek Symbol

α	Angle of Attack (°)
ρ	Density of Air (kg/m^3)
ω	Angular Velocity of Blade (rad/s)
Λ	Tip Speed Ratio

CHAPTER 1 Introduction

1.1 Introduction to wind energy

The ever-increasing gap between the demand and supply of energy shows that energy is one of the major concerns of the world today. This issue demands alternative, innovative and efficient solutions for producing electrical energy. Pakistan has a very large gap between this demand and supply and many areas have still not been electrified yet. Though Pakistan is using some indigenous sources like hydro-power and thermal power to generate sufficient electricity, the country still does not have enough grid capacity to store the generated electricity. Due to lack of development and research in the field of renewable energy, the country is forced to import fossil fuels for power generation which increases the burden on its economy. To overcome the energy shortfall, it is necessary to adopt methods using renewable resources like hydropower, solar and wind for generation [1].

1.2 Objectives

This final year project's objective is to design and model fabrication of the vertical axis Wind Turbine (VAWT) that can be used for testing and experiments and would serve as a basic model for a product to be commercialized. The objectives of this project include

- Design and the analysis of the blades of vertical axis wind turbine using low wind speed airfoils
- Comparison of CFD analysis of the vertical axis wind turbine with subsonic wind mill analysis.

1.3 Wind energy

Among the most economical sources of energy available today is wind. The wind's kinetic energy is converted by a wind turbine into mechanical work that powers a generator to provide electricity. Its efficiency depends on wind speed and higher altitude experience more speed. The average wind speed of offshore resources is 90% being land, most wind turbines are currently located at sea [2].

1.3.1 Local wind: Sea breeze

As the global winds are important in order to determine the prevailing wind direction in the given area, but wind directions are also influenced by the local climatic conditions. The sum of global and local effects is important in determining the wind direction because of this local wind is always arranged upon the largescale wind systems. Local winds may ascendant the wind patterns if the largescale winds are low. During daytime land masses heated more rapidly

than the sea. The low pressure that is created at ground level is mainly due to the air arises out to the sea and it also attracts the cool air from sea. It is called sea breeze. The land and sea temperatures are equal at nightfall and this is a calm period [3].

Figure 1 Sea breeze [4]

1.3.2 Troposphere

The ecosystem has skinny layer across the globe. The diameter of globe is 12,000 km. The area wherein all climate and greenhouse impact arise is eleven km altitude of troposphere. The given Figure indicates the stretch of approximately three hundred km of island throughout and the choicest peak of the troposphere. Let's examine a one of a kind angle, the diameter of ecosystem might be 1 mm if the globe have been 1.2 meters diameter of ball [5].
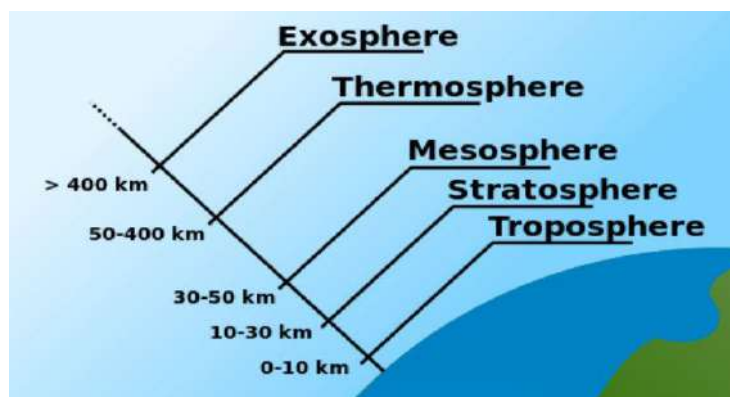
Figure 2 Various atmospheric layers across [5]

1.3.3 Geostrophic wind

Wind is driven mainly by temperature and pressure differences. It is called the geostrophic wind. There is almost no effect on the surface of the earth. That's al about 1000 meters above

13

the ground, you can see the geostrophic wind. The balloon Used to measure the velocity of geostrophic winds [6].

1.3.4 Forces that effect the wind

The forces that effect the characteristics of wind are

- Pressure Gradient
- Carioles Force
- Frictional Force
- Centripetal Force

1.4 Wind Obstructions

Trees, rocks, buildings and mountains, etc. influence the wind direction and speed causing irregular wind patterns due to turbulence in the wind. This turbulence is more around the obstacles and it may last to some three times the height of the obstacle. Turbulence is higher at the back of the object than in front of it. It is necessary to avoid those obstacles during installation of a wind turbine because it effects the speed and direction of the wind [7].

1.5 21st Century Wind Technology

Wind energy technology continues to flourish and grow in the present century as more and more emphasis is being laid in the environmental health and global warming and due to scarcity of fossil fuels as well. Floating wind turbines and offshore wind farms are a major break-through in the field of power and energy in present times. The commercial wind industry continues to grow at a rate of 25% per year and still has a lot of potential in it to meet the energy requirements of the world [8].

1.6 Types of Wind Turbines

Wind turbines are classified on various principles, for example on the principle of the axis of rotation of rotor blades, wind turbines have two types.

- Horizontal axis wind turbines
- Vertical axis wind turbines

On the basis of rotor placement relative to tower and nacelle:

- Up-wind
- Down-wind

On the basis of mechanism which the rotor blades use to attain the rotation and thus generate electricity:

- Lift type
- Drag type

Today, commercial turbines are three bladed, horizontal rotational axes with one rotor having lift type mechanism.

1.7 Horizontal Axis Wind Turbine

The HAWT, the very popular form of wind turbine available, is one of the essential types. You usually picture these kinds of wind turbines when you hear the word "wind turbine." The concept behind these turbines is essentially the same as that of windmills; rotor blades are attached to a shaft and move it as the wind blows across them; the difference is that this time the shaft is attached to a generator that generates the projected electrical energy. They resemble an enormous aircraft propeller positioned atop a pole or tower. A wind turbine with a horizontal axis is one type that must be aligned along the direction of the wind. They require a wind sensor to measure the wind's direction along with a yawning mechanism in order to be properly oriented against the wind. The need to face the wind stems from the need for a more efficient force distribution on the rotors as well as the need to prevent structural failure to the turbine from inappropriate stress on the turbine frame [9].

Figure 3 Horizontal axis wind turbine [9]

In terms of structural considerations, horizontal axis wind turbine structures must be sufficient in strength to withstand the weight of the rotor blades, gearbox, generator, as well as other turbine components. Moreover, the mast's base must be capable of withstanding the strong

15

winds that blow where the turbine is assembled. HAWTs are among the most widely utilized type of wind turbine because of their efficiency and relatively higher power generation ability for a similar footprint. These kinds of wind turbines are therefore used in the majority of wind farms, that are power plants that produce electricity from a number of wind turbines.

Horizontal - axis turbines are classified into two types: up-wind turbines and down-wind turbines. Let us go over each of them in more detail below [9].

1.7.1 Up-wind Turbines

The majority of wind turbines are of this type. With their backs to the wind, upwind HAWTs allow the wind to reach the rotors before the mast. Because of this, the rotors operate more effectively and are less sensitive to rotor wear and tear. Additionally, the wind shade beyond the tower is not a factor. However, the yawning mechanism's requirement adds to the structure's weight.

Figure 4 Up-wind turbine [9]

The rotors of up-wind wind turbines must not be elastic in order to avoid them from bending and colliding with the mast in high gusts, which is another factor to take into account. The rotor is positioned considerable distance from the tower in order to further prevent such occurrences. This makes it more challenging to manufacture these kinds of wind turbines, and the rotor blades' relative rigidity means that more material is needed to make the blades [9].

1.7.2 Down-Wind Turbines

The less common types of wind turbines are those with a downwind horizontal axis wind turbine. Their design is substantially the same as up-wind HAWTs, with the difference of the rotor's position, which is below the tower; the wind reaches the mast before it reaches the blades. This combination increases flexibility and allows for the use of lighter materials for the rotor blades. Therefore, this design achieves the dual goals of having a lighter weight of the structure and improved geometrical configuration of the tower by transferring most of the load from tower to the blades in their bending [9].
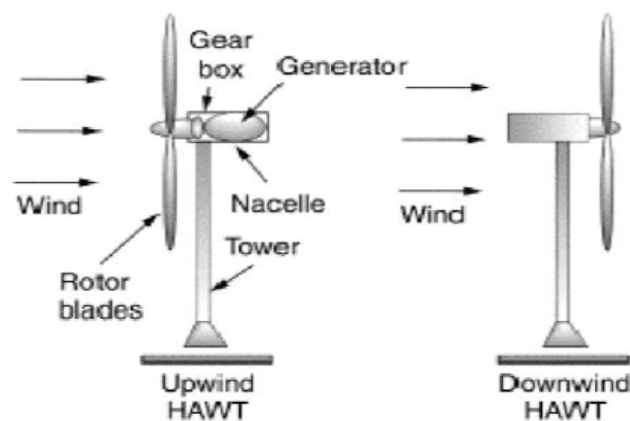
Figure 5 Up-wind and Down-wind turbine [9]

Theoretically, if the rotors and enclosures are designed so that the casing automatically follows the direction of the wind, down-wind horizontal axis wind turbines don't really require a yawning mechanism. The proactive yawning of these turbines would not help large wind turbines with earthing cables attached to the casing.

These wind turbines experience wind shading because their rotors are downstream of the tower and behind the mast. In addition to causing variations in the amount of power produced, wind shadow makes down-wind kinds of wind turbines work harder than their up-wind versions. [9].

1.8 Vertical Axis Wind Turbine (VAWT)

Vertical axis wind turbines are able of capturing wind from the all directions and need not to be directed into the wind. Initially, vertical axis designs required a power source to overcome its high torque for initial rotation. But recently, developments in the blade designs have lowered the torque values and thus, do not require any external power.

1.9 Types of VAWT

1.9.1 Savonius Wind Turbines

Savonius turbines are VAWTs of the drag type since drag is what causes them to rotate. Their concept is quite similar to that of cup anemometers. A cup facing the wind on a cup anemometer, like the one below, always having the maximum drag being applied to its surface, whereas other cups have other round, and hence drag-lowering, surfaces along the wind. The similar rule applies to what occurs in Savonius-style wind turbines. As shown in the graphic below, it is always only one surface which experiences the greatest drag however, others have quite less drag force applied to them [9].

Figure 6 Savonius turbine

The key feature of this model is that it would revolve regardless of the wind's direction. These particular wind turbines are also excellent at operating in low-speed winds, simple to make and maintain, and effective in turbulence. Despite these benefits, the design is incredibly ineffective. Because the favorable and unfavorable drag forces are not that dissimilar from one another, so the rotational speed would also not be as high.

1.9.2 Darrieus Wind Turbines

Contrary to Savonius wind turbines, Darrieus wind turbines belong to the lift-type VAWTs, for which the thought of airfoil lift production has also been adopted. These wind turbines have curved, C-shaped blades which extend from the tower's top to the bottom where they are attached to the shaft of generator, making them the most popular design of vertical axis wind turbines for generating power. They rotate at faster speeds, which might provide more power, and as a result they have good efficiency [9].

Figure 7 Darrieus turbine [9]

Higher rpm and less torque necessitate an external device of initiating procedure for such kinds of the wind turbines, like another Savonius turbine, for increasing the rotational speed to a point where these Darrieus blades may "hold the wheel." Additionally, they experience torque ripple, that is a cyclical increase and reduction in the produced torque and corresponding cyclical force onto the tower structure. The darrieus wind turbines with three blades do not have this torque ripple problem [9].

Darrieus Vertical Axis Wind Turbine are distributed into three types.

- H-Rotor VAWT
- Helical VAWT

1.9.3 H-Rotor VAWT

The wind energy converter under study is a VAWT, a less popular variety of wind turbine. Since the VAWT is an omnidirectional, it does not require a yawning mechanism and may accept wind by all directions. The VAWT is also anticipated to be quieter than a HAWT. The proposed design comprises a turbine having straight blades that are supported arms that are connected to the drive shaft. The term "H-rotor" is frequently used to describe this setup. The driving shaft is directly attached to the generator's rotor and is typically shielded by a tower and supported by guy wires.

19
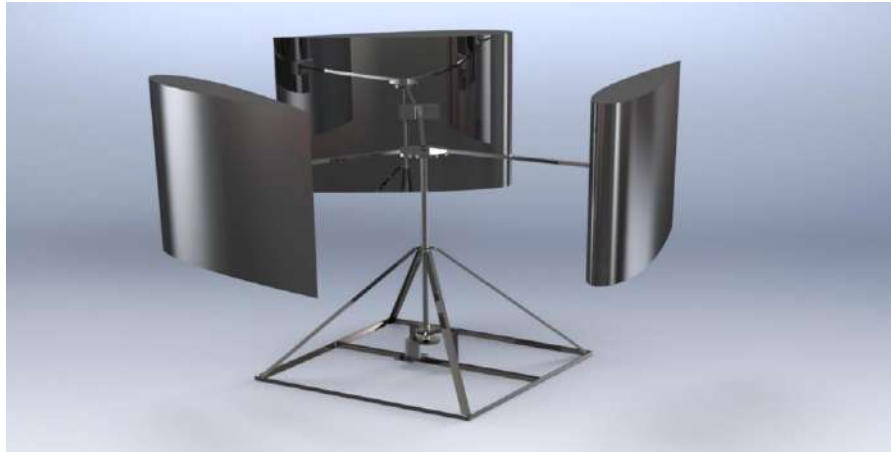
Figure 8 CAD model of H-Rotor VAWT

Chapter 02 Literature Review

2.1 Blade Design Selection

According to the study discussed in this article, NACA 0012 and NACA 0015 scored better in terms of force, velocity, and coefficients of lift and drag. NACA 0018 and NACA 0021 likewise performed admirably under the circumstances, but with significant drawbacks. Therefore, according to Shukla et al., the improvement employed was ideal for enhancing the performance of the NACA 0012 and NACA 15 airfoils. The best phenomenon was achieved by NACA 0018, which increased lift while reducing drag for the dimple-used airfoil. However, additional modifications succeeded in reaching higher values than the airfoil did. Additionally, their analysis demonstrated that for the NACA 0012 and NACA 0015 airfoils, the value of stall was low [10].

According to O. S. Gim et al., the flowing rates and profiles about the NACA 0018 foil at Re142.5 104 were used to verify the impact of an end plate affixed at the end-span. The 2-frame cross correlation PIV approach was used to view and measure the flow fields across the foil at various attack angles both with and without an endplate. In addition to taking into account the interaction with a ship's hull, propellers, and rudders, the overall forces of a foil that deal with complicated lift and drag forces would also be taken into account [11].

According to the research by S. Brusa et al., a wind turbine's power coefficient rises as the Reynolds number of the blade increases. The Multiple Stream Tube Model-based calculation code was used to demonstrate how the rotor solidity and Reynolds number have an affect on the power coefficient. According to geometry, as aspect ratio decreases, the Reynolds number increases, which enhances the efficiency of vertical axis wind turbines [12].

The NACA0018 airfoil was found to be the best suitable airfoil section for use in a vertical axis wind rotor in the journal (IOP conference series et al.), because it would allow the wind turbine to achieve the maximum value of wind energy utilization efficiency while also having a cheaper production cost in comparison to other designs. The aerodynamic shape of the blades ensures that they will settle in a direction at each of the four power extraction components. Straight blades with the NACA 0018 Airfoil section were employed in the design [13].

According to J.O. Dabiri et al., in order to generate wind energy, the site characterization required the inclusion of the following significant parameters and data: An average annual

wind speed (WAsP needed the wind information collected at every 10 minute pulses by an atmospheric mast in the similar area), the density of wind power, a wind rose, a map for wind resource, the predominant wind direction, the division and persistence in speed frequency, a vertical wind speed profile, and a wind shear exponent, Wei bull shape parameter (k), a scale parameter (c), the turbulence intensity, the density and variation of wind both vertically and periodically, historical wind information (along with frequency and potency of previous storms) etc [14].

Three techniques were employed by R. G. J. Flay et al. to analyze the behavior of the wind flow across the naturally complex topography of the Belmont Hill, which is positioned close to Wellington, New Zealand. The experiment for wind tunnel was conducted at a scale of 1:2000, and the CFD algorithms were used to construct the 3D numerical assumptions of the terrain [15].

According to Moshfeghi et al., the split blades had a favorable impact on the turbine's ability to generate power at top speed ratios lower than 3.5. Under this range, the power produced by a blade with a split that runs from the root of the blade to a spot near the tip increased by up to 48%. Additionally, the split's impacts on the power generation are stronger when it is placed in an outer radial position [16].

Wind turbine BEM (Blade-Element Momentum) analysis has been carried out using the free software Q-Blade to analyse NACA 0018 by R. D. Ionescu et al. The 150000 and 300000 Reynolds numbers were used in the analysis. The tiny readings for flaps deflection up to 20 degrees (2,5 and 10 degrees) (2,5 and 10 degrees) display a rising C L/C D ratio, and they were suitable for assisting the wind turbine's self-starting [17].

According to R. Corniglion et al., the dynamic inflow models were frequently employed to simulate the unstable aerodynamics for floating offshore wind turbines, even though these models were designed for blade pitch variations rather than floater motions. In this instance, the two scenarios for which dynamics inflow was practically observed—the blade pitch and the rotor speed steps—were contrasted with a simple condition, a surge velocity step. Both a rise and a decrease in the coefficient of thrust, were compared with the change of the thrust coefficient with alterations in blade pitch, speed of rotor, and the surge step estimated using the FVW method. The thrust coefficient overshoots with a delay before reaching the steady output that is proportional to the new operating circumstances as a result of the changes in the rotor speed and pitch of the blade. This was the dynamic influx effect. It was recently

discovered that the virtually quasi-steady loaded variation for a harmonically surge wind turbine that did not display a significant dynamic behavior for the surge case of the thrust coefficient, that incorporated the additional velocity owing to motion for its normalization [18].

The analytical helical vortex model, as described by D.B. Araya et al. in the article, it demonstrated that with the three perturbations, the majority of the blade exhibits a temporal behavior that is strikingly similar to that at the centre of the rotor, where a closed-form transition occurs. The induced velocity could be easily calculated using the helical vortex model everywhere in the domain, but especially at the inter-blade point. While Berger et al.21 found experimentally that the temporal behavior in case of the blade pitch was similar at r=R 14 0:9 and r=R 14 0:6 on the inter-blade position, the position located at the top showed a rapid temporal reaction at the blade position because of the quick contribution of the top vortex. This is in favor of using smaller time factors around the very edge of the blade in variable inflow models for BEMT, along with the time constants remaining relatively constant for most of the time period [19].

Three distinct rotor configurations for the VAWT model were suggested by M. Anthony et al. for a low wind metropolitan region. It was established in the ANSYS Fluent software as a realizable k-ε turbulence model. For all three variable rotor designs, this model provided more accurate findings and improved convergence characteristics. The postulated WFM-based VAWT design increased the velocity of the wind in its outlet prior it approached the blades of turbine, according to the simulation findings. It could have the following advantages [20].

According to P.L. Delafin et al., five distinct turbines depending on the Sandia 17-m vertical axis wind turbine, utilizing two, three, and four blades, were studied. A vortex model was developed to estimate the power of coefficient and instantaneous torque, thrust, and the lateral forces [21].

G. Diwakar et al., explained in the study that efficiency was calculated using Output energy of turbine and input energy of wind. Variation of efficiency with respect to blade angle was observed. Finally, it was concluded that when the angle between the blades is 30 degrees the efficiency was high when compared to remaining angles. It was observed that VAWT is good for lower wind speed. Turbine blades were designed with flat, curved and S-shape. The material used was aluminum. After comparing the result of stress with different shapes of blades, flat blade shape was effective when compared to other blades. The von missed stress values for flat

blade are 6.265(max) and 0.521E-07(min). Hence it recommended to use flat blade for getting higher efficiency values if the wind direction is only one side [22].

An original utilization of circulation control technique to vertical axis wind turbine (VAWT) blades was described by A. shires, V. Kourkoulis, et al. In order to provide an appropriate performance during upwind and downwind cycles, the aero-foil structure must be compromised because a VAWT rotor's blades had a variable attack angle during its rotation. As a result, VAWT blades were often cambered airfoils designed to enhance horizontal axis wind turbine rotor efficiency rather than symmetrical airfoils with a reduced lift-to-drag ratio. Circulation control (CC), also known as the use of a tangential air jet to boost lift by dispersion and jet incorporation, was a rather advanced technique. However, very few academics have thought about using it to better the performance of wind turbines. This study examined the viability of the technology by first analyzing performance trends of several CC airfoils using computational fluid dynamics (CFD), and then analyzing VAWT rotor efficiency including these CC airfoils by using a blade component momentum-based framework [23].

According to A. Siddiqui et al., this report described how an experimental facility created to perform experimental investigation and evaluation of wind turbines was constructed and successfully used. The configuration allows for testing vertical-axis wind turbines. Three alternative setups—setups A, B, and C—were used to evaluate the hybrid VAWT. The Savonius rotor was positioned in the center of the Darrieus rotor in setup A, just above Savonius rotor in setup B, and at the top of the Darrieus rotor in setup C. In every example examined for this investigation, the hybrid system outperformed the Savonius or Darrieus turbines individually. Additionally, it was discovered that the setup delivered superior outcomes to other combinations [24].

2.2 Numerical studies on wind turbines

The goal of the work by M. Balaji et al. was to increase the performance of the H-rotor Darrieus, including its efficiency and operating range. Using 25 varying airfoils, a numerical inspection of a three-bladed Darrieus rotor was performed. Transient RANS computations and a comprehensive examination of simulations have been presented for various values of the turbine speed ratio. It has been researched to learn the power and torque output coefficients of the turbines as well as the various forces acting on the turbine components. Additionally, rotor performance was compared to and associated along with the data from earlier study that utilized the NACA 0021 airfoil [25].

M. Richmond proposed using the actuator disc method to perform a fluid dynamics computational analysis of an operating wind farm. These instances were not only run at various wind speeds and directions, but the outcomes were also correlated to actual data that was recorded at the wind farm. In order to make the method followed repeatable, the open-source code Open FOAM was employed, and modifications to the scripts were shown. Furthermore, techniques for processing the data from the wind farm are provided. For all simulations, the two turbulence models, one standard k-ε and the other k-ω SST, were investigated [26].

R.G.J. Flay et al. investigated the behavior of the wind flow through the naturally complicated topography of the Belmont Hill, which is located close to Wellington, New Zealand, using three different methods (observations, wind tunnel, and numerical). The test for wind tunnel was run at a scale of 1:2000, and full-scale CFD simulations of the topography using the Gerris and WAsP codes were done. Nine 5 meters high cup anemometer field data were evaluated with the outcomes of the computer modelling and the wind tunnel study. All approaches produced similar results, with WAsP producing the worst agreement [15].

According to L. Wang et al., this study used computational fluid dynamics and finite element analysis to create a fluid structure interaction (FSI) framework for horizontal-axis wind turbine blades. The coupling technique applies the aerodynamic charges established by CFD to FEA modellings as load initial conditions depending on only one coupling. The FSI model was employed to the FSI simulation of the 1.5 MW WindPACT wind turbine blade, a typical of relatively large-scale horizontal-axis wind turbine blades, and was validated by a number of standard computational experiments [27].

The implications of the split's location along the span on aerodynamic performance, the power production, and flow patterns across a HAWT were numerically examined by M. Moshfeghi et al. Five distinct split configurations and the NREL Phase VI CER blade without split were simulated at various top speed ratios ranging from 2 to 6 (corresponding to wind velocities from 20 m/s down to 7 m/s). The unstable SST-k-ω turbulence model has been used in the CFD simulations. The split blades had a favorable impact on the turbine's ability to generate power at top speed ratios lower than 3.5, according to the results [16].

According to M.M. Elaska et al., the spread of the AOA over the course of the cycle has a considerable impact on the VAWT's overall power coefficient, making accurate AOA estimate crucial. It was discovered that employing the flow data collected from two referral points at the different positions 0.5 aerofoil chord lengths upstream, and one chord away by each side of the

aerofoil can give the most precise assessment across a variety of operating conditions. This is because the flow across the VAWT is extremely complex. With the new approach, the AOA data would be calculated and stored during CFD simulations without any need for time-consuming post processing [28].

According to M. Hassanpour et al., the performance and flow behavior of a system consisting of two similar straight blade vertical axes wind turbines were evaluated. Three parameters were examined: the angle of an incoming wind (β), the vertical line among the mid-heights of the two wind turbines (h), and horizontal displacement between the axes of the two wind turbines (S). Through nine numerical experiments, the simultaneous effect of design variables was investigated using a fractional model of the experiment depending on the Taguchi's L9 orthogonal array. Three-dimensional numerical tests were carried out by using the computational fluid dynamics (CFD) tool, ANSYS Fluent. [29].

According to L.R. Amjith et al., wind turbines are largely utilized to generate electrical power without relying on fossil fuels, which are running out. This project involved the design and computational analysis of a 5 MW horizontal axis wind turbine blade. Solid Works program was used in the design of the blades. In ANSYS Fluent, the evaluation and post-processing were completed. Each blade's attack angle was adjusted from 0-90 degrees, and the related lift values, drag force, and momentum values were computed [30].

According to P. Negi, M. Subhash, and colleagues from this study, analysis was done in ANSYS 15.0 FLUENT by varying the angle of attack on S809 airfoils both with and without slots. The upper boundary layer was going to be energized and attempted to pull flow separation down towards the trailing edge by employing leading edge slot. Results from S809 aerofoils with and without leading edge slots were examined to see how the changes in drag and lift affected the aerodynamic performance. The findings were obtained at various angles of attack between 0 and 30 degrees [31].

Aeroelastic performance investigation of the HAWT swept blades under the yaw angles of 0, 10, 30, and 60 at wind speeds of 10 m/s was carried out using the ANSYS Fluent for CFD evaluation and the Static Structural for FEA, according to S. K. Thangavelu et al. Investigation and comparison of the impact of yaw error on swept and unswept blades aeroelastic performance were carried out. The findings demonstrated that yaw error, as predicted, has a negative affect upon the aeroelastic performance of the swept blades and exhibits a comparable pattern for unswept blades. In light of the findings, it can be said that the swept blades perform

better aero-elastically than unswept blades in context of higher rotor power and less deformation, or greater stability under yaw conditions [32].

The impact of the Gurney flap, dimple, and their combination was demonstrated by V. Shukla et al. using a variety of VAWT aerofoils (vertical axis wind turbine). They achieved positive results for various conditions and aerofoils by using a consistent Reynolds number value to assure the uniformity of velocity for all blades. One of the best adjustments made in recent works was the introduction of dimples in the aerofoil. However, they observed in their investigation that the dimple's performance was not nearly as successful as other aerofoil changes. The lift (CL) obtained by the dimple aerofoil was less than that of the plain blade and experimental data for all types of aerofoils they employed. Although it was less than the other values, it was higher than the maximum value mentioned in aerofoil NACA 0012. When using the NACA 0018 profile at an angle of attack of less than 140, an aerofoil with dimples might achieve its maximum speed [10].

According to M. Balaji et al., the main focus of their simulation-based study was on the same butterfly valve's abrupt pressure drop at different valve opening angles as well as the existence of backflows, which have a negative impact on the flow across the throttle body. Data gathered from the experiment were compared with the results from the simulation. Similar to the experimental data, the flow modelling revealed that the pressure difference across the rectangular shaft profile was lower than that over the circular profile [25].

High-fidelity URANS simulations that were verified with experimental data were used to extrapolate the research of S. Sahebzadeh et al., into the impact of relative spacing (i.e., a relative distance and an angle) on the single and collective power performance of the two co-rotating, and co-phase turbines in a dual rotor VAWT configuration. The study encompassed a large range of numbers for relative angle ($-90\circ \leq \Phi \leq +90\circ$) as well as relative distance ($1.25d \leq R \leq 10d$). Regarding the upstream turbine: - For R/d ≤ 2.25 at $-45\circ \leq \Phi \leq +30\circ$, the power coefficient decreased to at least 90% of the isolated solo turbine (CP Solo). The drop is because of the upstream induction of the downstream turbine (TurbII). - Outside the aforementioned region, the effect of TurbII on CP TurbI was limited to < 5 and below 2% for R/d ≥ 5 [33].

The efficiency of a 5kW three-bladed H-rotor Darrieus VAWT with cambered TLE NACA 0025 blades was determined by I.C.M. Lositano et al. using CFD. Using CAD and CAE tools, 3D VAWT designs were created, and simulations were run. Then, utilizing post-processing analysis integrating the flow visualizations with different torque assessments, lift and drag

characterization, and other techniques, the physics of the VAWT and blade flow were covered in detail. To get convergent findings, transient steady wind flow simulations utilizing the k-ω SST turbulence design required 10 full VAWT rotations each. Throughout the simulations, the lift, drag, and moment coefficients on each of the three blades were tracked separately [34].

The primary goal of this work by M. H. Mohamed et al. was to enhance the performance of the H-rotor Darrieus, including its efficiency and operating range. Using 25 various airfoils, a numerical analysis of a three-bladed Darrieus rotor was performed. Transient RANS calculations and a comprehensive examination of simulations have been introduced for various values of the turbine speed ratios. It has also been researched to learn the torque and power output coefficients of the turbines as well as the various forces acting on the turbine components. Additionally, in order to validate the current model, rotor performance has been compared to and recognized with a previous work result using the NACA 0021 airfoil. To identify the best sectional airfoil that may be employed in a Darrieus turbine, the power and torque coefficients were both derived as a function of the blade speed ratio [35].

Through the use of a PARSEC approach, Taguchi algorithm, and CFD simulation, J. Chen et al. conducted a thorough analysis to identify the ideal airfoil for VAWTs in this paper. In contrast to other studies, the PARASEC approach was chosen because it offers a wide variety of design options and covers a large portion of the airfoil form space. Additionally, they changed the PARASEC approach so that its 12 design alternatives were directly tied to the geometric parameters, making it more intuitive from a geometric standpoint than other methods. Additionally, the PARASEC approach would be altered to make asymmetric airfoils by designing the upper and bottom surfaces differently. The Taguchi algorithm was used to select the solutions with the least amount of work while identifying the impact weight for every parameter and locating the key geometrical parameters. They also performed SN analysis, contribution ratio computation, and the impact of design changes on the power coefficient [36].

The findings of LES computations on a VAWT were discussed in a publication by A. Posa et al., which also discussed the sensitivity of wake parameters to TSR using ensemble averaged and phase-averaged statistics. Cartesian grids with around 1 billion nodes were used for simulations. By comparing the overall strategy with PIV readings from the wind tunnel, the same flow problem, the general strategy was validated. Additionally, it was discovered that all findings were in strong agreement with previous experimental research. Calculations showed a bigger result [37].

The goal of H. Day et al.'s study was to develop a low-cost optimization procedure by applying potent adjoint procedures to the problem of VAWT aerodynamics. Due to a lack of literature on the subject, a semi-transient ad-joint based optimization procedure was created. To prove its viability, it could only employ one adjoint solution (or "snapshot") every turbine revolution. A number of variations of the procedure were tried using the optimization process on a typical turbine with a TSR of 4.5. The results show that the optimizing VAWT blade shape with a steady Adjoint solver and unsteady CFD simulations can be done with just one Adjoint snapshot per revolution [38].

M. Kumar et al. found that after adopting wind turbines designed to be proposed on the centre of the Bhopal-Indore highway, wind energy was produced through the wake of moving vehicles on both sides of the highway. However, for increased power generation, we positioned an array of VAWT on the middle of a highway. Waste material was used to create a four-bladed VAWT, and no modification on the turbine blade's aerodynamic geometry was required because, after trimming the plastic drum, the VAWT resembles a Savonius design. This kind of VAWT is also constructed by the untrained individual to meet his energy needs [39].

Chapter 3 Methodology

3.1 Design Calculations of VAWT

We designed an H-rotor Vertical-Axis Wind Turbine (VAWT) that would generate power under relatively lesser wind velocities. We worked on the SolidWorks for 3D CAD model. The available wind velocity is 3.88m/s on the roof of department of Mechanical Engineering of KFUEIT (Rahim Yar Khan). The following equation is used to denote the wind power:

$$P_o = \frac{1}{2}\rho AV^3 \tag{3.1}$$

where

A= Swept Area $= H \times D = 0.8 \times 0.5 = 0.4 m^2$

$\rho = Density = 1.225 \, kg/m^3$

V= wind velocity = 3.88m/s

$$P_o = 14.31W$$

Swept area for vertical axis Wind Turbine is measured by the multiplication of the rotor height, 'H' and rotor diameter, 'D'. The larger the swept area, the larger would be the power generated.

$$A = D \times H \tag{3.2}$$

$$A = 0.8 \times 0.5 = 0.4 m^2$$

In the case of zero aerodynamic losses as well as other losses during the power conversion operations, the wind power in Eqn. (3.1) reflects the optimum power of a wind turbine. All energy cannot, however, be transformed into beneficial energy in this way. The Betz limit refers to a wind turbine's optimal efficiency. Only 59.3% of the wind energy can, at best, be transformed into usable power, as determined by the Betz limit. The gearbox, bearings, generator, transmission, and other components could all lose some energy. The H rotor's maximum power coefficient, Cp, is 0.30. Therefore, 0.30 is the Cp value employed in this project. The power output when the power coefficient is taken into account is:

$$P = \frac{1}{2}\rho AV^3 C_p \tag{3.3}$$

where

$$C_p = 0.3$$

$$\rho = \text{Density} = 1.225 \text{ kg/m}^3$$

V= wind velocity = 3.88m/s

$$P = 4.293\text{W}$$

3.2 Power at Shaft

Maximum power at shaft is

$$P_T = C_p \times P_o \tag{3.4}$$

$$C_p = 0.3$$

$$P_o = 14.31W$$

After putting values in formula, we get

$$P_T = 4.293W$$

3.3 Tip speed ratio (T.S.R)

The difference between both the tangential speed of a blade's tip and an absolute speed of the wind is known as the tip-speed ratio (TSR), λ, for wind turbines. The tip speed ratio for a well-designed turbine structure is from 6-8. For a common or for not a well-designed turbine tip speed ratio is 5-6.

T.S. R= λ=5

3.4 RPM at Shaft

$$N = \frac{60v\lambda}{\pi D} \tag{3.5}$$

Then by putting values

N = 436.36 rpm

Now for rotational speed Ω

$$N = \frac{60\Omega}{2\pi}$$

As

$$\Omega = \frac{2\pi N}{60} \tag{3.6}$$

So

$$\Omega = 45.67 \text{ rad/s}$$

3.4.1 Maximum Torque at Shaft

Maximum torque is

$$T_{max} = F_{max} \times R \tag{3.7}$$

Where R is the radius of the turbine

$$R = \frac{V\lambda}{\Omega} \tag{3.8}$$

Maximum thrust available to turbine is

$$F_{max} = \frac{1}{2}\rho A V^2 \tag{3.9}$$

Then maximum torque becomes,

$$T_{max} = \frac{1}{2}\rho A V^2 \times \frac{V\lambda}{\Omega}$$

As power in the wind is

$$P_o = \frac{1}{2}\rho A V^3$$

So maximum torque at the shaft is

$$T_{max} = P_o \times \frac{\lambda}{\Omega} \tag{3.10}$$

where

$$P_o = 14.31W$$

$\lambda = 5$

$\Omega = 48.5 \text{rad/s}$

$$T_{max} = 1.475Nm$$

3.4.2 Torque at Shaft

$$T = T_{max} \times C_T \tag{3.11}$$

where

C_T= Torque Co-efficient

And

$$C_T = \frac{c_p}{\lambda} \tag{3.12}$$

We got the value of torque coefficient from this equation that is

$$C_T = 0.06$$

Then torque T becomes

$$T = 0.06 \times 1.475$$

$$T = 0.0885 Nm$$

3.5 CAD Design of a Vertical Axis Wind Turbine

The Figure shows the CAD model of H-Rotor VAWT

Figure 9 CAD Model of H-rotor VAWT using SolidWorks

H- Rotor VAWT have the following components:

- Blade

- Airfoil
- Shaft
- Radial Arms
- Support
- Screws

3.6 Materials used for Vertical Axis Wind turbine

Wind turbines are mostly manufactured of steel (66-79% of the overall turbine mass), fiberglass, resin, and plastic (11-16%), copper (1%), iron or cast iron (5-17%), and aluminum (0-2%), according to research from the National Renewable Energy Laboratory.

The United States imports and manufactures a large number of turbine parts. The Office of Energy Efficiency & Renewable Energy's Land-Based Wind Market Report states that nacelle assemblies (85%), blade and hub components (30-50%), and wind turbine towers (60-75%) are all obtained domestically to a greater or lesser extent. But a lot of internal components, like pitch and yaw systems, axles, screws, and controllers, are frequently imported [40].

3.7 CAD Design of Airfoil Blades

We use three blades in our project. The length of one blade is 800mm. We use 3 blades because having minimum number of blades reduces drag. The shape of blade is shown in solid work.
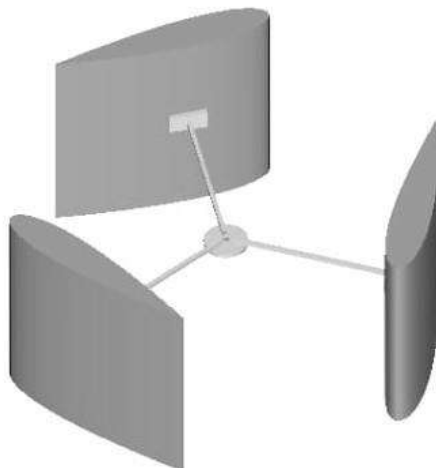

Figure 10 3D model of the Blade

3.7.1 CAD design of Radial Arms

Radial arm is the distance between center Airfoil and the shaft. Some specific systems are used to assemble or dismantling of airfoil and shaft such as nut and bolt. With the help of reference

circle, we draw redial arms for our blade from the center as shown in figure. We selected mild steel bar for making radial arms. For our project, we have accepted a 250mm length for each arm by approximating the length to the size of the rotor.
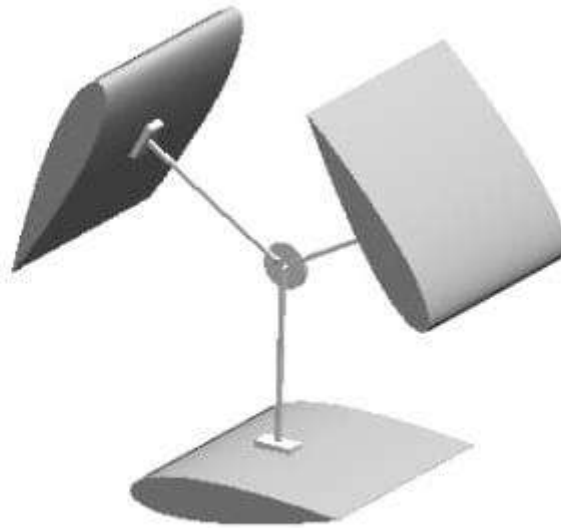

Figure 11 Radial Arms connected with Airfoil Blades

Table 3-1 Description of Radial Arm

Serial No	Description
1	Arm Number (3)
2	Arm length(250mm)

3.7.2 CAD Design of Shaft

A spinning machine component called a shaft is used to transfer power from one location to the other. The power is transferred to the shaft by the tangential force, and a torque created inside the shaft then enables the power to be sent to different machines that are connected to the shaft. The different devices, such as pulleys, gears, etc., are mounted on it for transferring power from one shaft to the other. The rotation of the shaft is caused by such parts and the forces which are applied to them. In other words, the shaft is responsible for transmitting the torque and the bending moments.

3.7.3 Materials Used for Shaft

The following qualities should be present in the shaft-making materials:

- Good machinability

- Higher strength

- Better heat treatment characteristics

- Lower notch sensitivity factor

- High wear resistant properties

Table 3-2 Shaft Dimensions

Serial No.	Description	Dimensions
1	Outer diameter of the shaft (mm)	27
2	Inner diameter of the shaft (mm)	21
3	Length of shaft (mm)	1067

3.8 Design Calculations of Shaft

Power of shaft is represented as

$$P = \frac{2\pi NT}{60}$$

where $T = Wr$

and $W = W_1 + W_2 + W_3$

suppose $W_1 = W_2 = W_3$

then $W = 3W_1$

where $W_1 = 1.5 kg = 1.5 \times 9.81 = 14.715 N$

$$W = 3 \times 14.715 = 44.145 N$$

and $r = 0.25 m$

$$T = 44.145 \times 0.25 = 11.03 \text{ Nm}$$

Taking N=100 rpm

$$P = 115.5 \text{ W}$$

Shear stress acting on the hollow shaft is calculated by

$$T = \frac{\pi}{16} \tau d_o{}^3 (1 - k^4)$$

Where T=11.03N

$d_0 = 0.027m, d_i = 0.021m$

$$k = \frac{d_i}{d_0} = \frac{0.021}{0.027} = 0.8$$

So
$$\tau = 4.85 \ MPa$$

Compressive stress acts on the hollow shaft is

$$\sigma_C = \frac{P_C}{A}$$

And $P_C = Weight \ of \ 3 \ Blades + Weight \ of \ 3 \ Radial \ Arms$

$$P_C = 44.145 + 4.905 = 49.05N$$

Where Cross section area of the hollow shaft is

$$A = \frac{\pi}{4}\left(d_o^2 - d_i^2\right)$$

$$A = 2.2608 \times 10^{-4} m^2$$

So compressive stress is

$$\sigma_C = 0.216MPa$$

Here the tensile stress of mild steel is

Tensile Yield Strength = 247MPa

Shear yield strength is represented by

$$Shear \ yield \ strength = \frac{Tensile \ yield \ strength}{2}$$

$$Shear \ yield \ strength = 123.5 \ MPa$$

Allowable shear stress is

$$Allowable \ shear \ stress = \frac{Shear \ yield \ Strength}{Factor \ of \ Safety}$$

Factor of safety is 9 in mild steel for live load. So,

Allowable Shear Stress = 13.72MPa

$$13.72 > 4.85$$

As allow able share stress for mild steel is 13.72MPa and our calculated value is 4.8MPa hence the Design is safe

3.9 CAD Design of Screw

A screw is such a device that transforms the rotational motion and torque (a rotational force) into a linear motion and a linear force, respectively. It belongs to the group of six traditional basic machines. The most typical design is consisted of a circular shaft with some external threads, which are helical ridges or grooves. The screw is inserted through a hole in some other material, the threads of which mesh with those on the interior of the hole.

Many screw threads are made to connect with an internal thread, which is a complementary thread. It typically takes the shape of a nut or another object with an internal thread molded into it. Different screw threads are made to create a helical groove as the screw is put in a softer material. Screws are most frequently used to place objects and hold things together.

Table 3-3 Screw Dimension

Tall (mm)	40
Diameter (mm)	6

3.10 CAD Design of Bearing

Dimensions of bearing are shown in Table 4

Table 3-4 Bearing Dimensions

Inner diameter (mm)	25
Outer diameter (mm)	52
Bearing Width (mm)	15
Type	Ball
Universal	6205

A particular kind of rolling-element bearing known as a ball bearing promotes motion by performing three key tasks:

- it transports loads,
- lessens rubbing

- places components of moving machines. In order to lessen contact area and friction along the moving planes, and the ball bearings use balls to differentiate the two "races," or bearing rings.

The bearing is also used to allow constrained relative movement between two sections, typically rotational or linear movements. In our project, we will utilize bearing sort 6205 that has the inner diameter is 25 mm.

Figure 12 Bearings used in the turbine assembly

3.11 Manufacturing of VAWT

3.11.1 Manufacturing of Airfoil Blades

Manufacturing process of Radial Arms and Airfoils has started by purchasing bar, metal sheet. Roller has been used to bend the metal sheet for making the Blade. Airfoil is the most important part of Wind Turbines. Because the power extracted from the air is totally depended upon the shape, size and number of Blades. The specific shape of Blades is called Airfoil. We have selected NACA-0018. For the fabrication, Stainless steel metal sheets were used. Because stainless steel has the following properties

- Resists corrosion.
- Strong tensile capacity.
- Very robust.
- Resistant to temperature.
- Simple manufacturing and formability.

- Long-lasting little maintenance

- Appealing appearance

- Recyclable; friendly to the environment.

For the fabrication, stainless steel metal sheets were used. Because this material has more ductility and strength and also low in weight. We fabricated three blades in a total. First of all, Plywood was used to make NACA-0018 profile. Keeping in mind the weight effect, we develop an idea to wrap up the wood profile with the metal sheets. We used three Plywood NACA-0018 profile in one Blade of Wind Turbine. One Plywood NACA-0018 is placed in the center of sheet and other two were joined at the both outer ends of the Blade. The Plywood and the sheet were joined by nails and rivets. The mechanical fastener usually known as a rivet is used to attach two or more pieces together. It also has an unthreaded plane shaft. This rivet cannot be separated from the hole due to permanently formed heads on both of the ends. Their components can't make a move radially due to the shaft. Total height of Blade is 0.8 m. Here chord length is 0.254m. All three Blades were fabricated in this fashion.

Figure 13 NACA 0018 Plywood Profile

We have used stainless steel metal sheet and Plywood. For pressing the metal sheet of the Blade, we have used hydraulic press. But before that, sheet is being cut to the calculated length. Then one side of sheet was pressed using the hydraulic press.

Figure 14 Cutting and Pressing of Metal sheet

Figure 15 Radial arm

3.11.2 Manufacturing of Shaft

In our design, we purchased a Shaft that is made up of mild steel. We did not compromised on standards and got the Shaft from a hardware store. We used mechanical workshop for rolling process to fit the ball bearing at its one side, while performing this process we kept in our mind that it requires a high level of accuracy.

Selection of Shaft is also a significant component of VAWT. Mild Steel Hollow Shaft was selected for the VAWT. Internal diameter of shaft is 21 mm and outer diameter is 27 mm. This Shaft was selected after the proper calculation and its availability.

- Material selection have been considered in calculation

- Stresses on the Shaft due to mounting of Blades and Hub on the top of the Shaft

- Chosen Shaft can bear the compressive stress as well as avoid failure due to buckling

- Shaft of 1.07m in length is used for VAWT

Figure 16 Manufacturing of Shaft

3.11.3 Manufacturing of Hub

Now the task was to join the all three blades with the shaft. For this purpose, we designed a hub. A circular plate type hub was fabricated by using mild steel material. Circular plate has the radius of 10.16 cm. Central hole has relative size to the outer size of the shaft of the vertical axis wind turbine. Proper machining work was done to make hub. On the plate we drilled three holes. These holes were drilled equally spaced or on 120 degrees in term of angles.

Figure 17 Manufacturing of Hub

3.11.4 Manufacturing of Gear System

Available DC motors in the markets have different or some standard specifications. If there is deficiency in rpm then to compensate it, we need to use gear box. To increase the RPM of the Shaft, we need to use Gears. Here Spur Gears were used. These Gears have 1:6 ratios. One rotation of Shaft will produce the 5rotation on the DC motor. Driver Gear has 54 number of teeth and the Driven Gear has 9 number of teeth. Pitch of the Gears kept small to get more smoothness.

Figure 18 Bevel Gears

3.12 Manufacturing Process Classifications

3.12.1 Deformation

- **Rolling**

Rolling is a process that reduced the thickness of the object. Diameter of the shaft is changed at the lower part from this process.

Figure 19 Rolling process on shaft

- **Filing**

As a finishing process, we use filing to remove unfinished materials. By this process, surface becomes smoother.

Figure 20 Filing process on shaft

- **Boring**

Boring process is used to enlarge the hole after Drilling. We used this process in Radial Arms and Center Plates to increase the diameter of the hole.

Figure 21 Boring process on hub

- **Punching**

It is a shaping procedure where a tool is forced by the punch press. This process is used for marking the holes before drilling process. We use center punch for marking before Drilling process on the Radial Arms.

Figure 22 Punching on sheet

- **Stamping**

We use Gas Cutter to heat the Radial Arms and then hammered the Radial Arms. Stamping process was needed at the both sides of Radial Arms to get the required shape.

Figure 23 Stamping on radial arm

3.12.2 Sheet Metal

- **Bending**

It is a process in which metal sheet can be deformed when we applying a force to the metal sheet. We applied force on stainless steel metal sheet to get the required shape of Airfoil Blades through this process.

Figure 24 Bending of aerofoil sheet

- **Drawing**

This is a forming procedure in which a punch is used to mechanically drag a blank metal sheet into a forming die. We put the Arm dimensions and Airfoil wood profiles coordinates on the metal sheet.

Figure 25 Drawing according to dimensions

3.12.3 Machining

- **Drilling**

Drilling holes for Screws and threaded Bolts installing. This process was done on the Radial Arms, Hub and Center Plate.

Figure 26 Drilling process on hub

- **Facing**

Facing is the process used to remove the material from the object. This process was done on the shaft to remove the extra material.

Figure 27 Facing process o shaft

3.12.4 Assembly

- **Riveting**

Installing the Radial Arms and Airfoil Blades by permanently fixing them with each other using screws.

Figure 28 Riveting on aero foil

Final shape of the project

This is how our project will ultimately look after all the steps are complete.

Figure 29 final shape of the project

Cost of Components of VAWT

Table 3-5 cost of components of VAWT

Part	Material	Quantity	Cost (Rs.)	Supplier
Shaft	Mild Steel	1	2000	Hardware Store + Manufacturing
Blade	Wood + Metal Sheet	3	6000	Manufacturing
Generator		1	4000	Hardware Store
Radial Arms	Mild Steel	3	900	Hardware Store + Manufacturing

Machine Screws	Stainless Steel	30	400	Hardware Store	
Gear System	Steel	2	5500	Manufacturing	
Bearing	Chrome Steel	1	2000	Hardware Store	
Hub	Mild Steel	1	2000	Manufacturing	
Other Cost			10000		
Total			32800		

Components required for testing of VAWT

We needed some equipment, such as a wind tunnel, a DMM (Digital Multi-meter), a tachometer, and an anemometer to measure the power of a Vertical Axis Wind Turbine when it was being tested.

DC Motor

A permanent magnet DC motor can function as a generator. It operates according to Faraday's Law. A conductor will produce electric voltage and current when rotated in the spirit of a magnetic field. We must give the generator the right rpm and torque in order to produce the necessary output. A vertical axis wind turbine's generator is a DC motor with variable voltage. Up to 24V can be produced by it. The DC-motor has a low RPM. We may change the voltages by adjusting the RPM.

Figure 30 DC Motor

Chapter 4 Numerical Simulation based study of NACA 0018

4.1 Introduction to NACA 0018

The National Advisory Committee for Aeronautics (NACA) produced NACA airfoils, which have the airfoil shapes for aircraft wings. The word "NACA" is followed by a string of numerals that describe the shapes of airfoils of the NACA. The numerical code's frameworks can be used to precisely create the airfoil's cross-section and compute its characteristics.

NACA profiles are divided into many types but major are 2 which are explained below;

4.2 NACA 4-digit Series

The four-digit NACA wing sections outline the profile as follows:

- The first digit is the chord's highest camber as a proportion.
- The second figure, in tenths of a chord, indicates the greatest camber from the airfoil sharp end.
- The airfoil's highest thickness expressed as a percentage of the chord's last two digits.

For instance, the NACA 2412 airfoil has a maximum depth of 12% of the chord and a maximum possible camber of 2%, both of which are positioned 40% (0.4 chords) from the top edge.

The NACA 0015 airfoil is symmetrical and lacks camber, as indicated by the 00. A number 15 denotes that the airfoil has a chord length to thickness ratio of 15%, meaning that it is 15% as thicker as it is long [41].

4.3 Procedure of Numerical based analysis of NACA 0018

1. Selection of NACA profile

The first step was to choose the NACA- profile, and for that NACA 0018 has been selected and data has been copied to the Excel file.

2. Import data to design modular

Then by importing the data of the profile into excel file and by specifying the co-ordinates import the data to design modular. Next step was to draw the profile, by using different commands the blade was made.
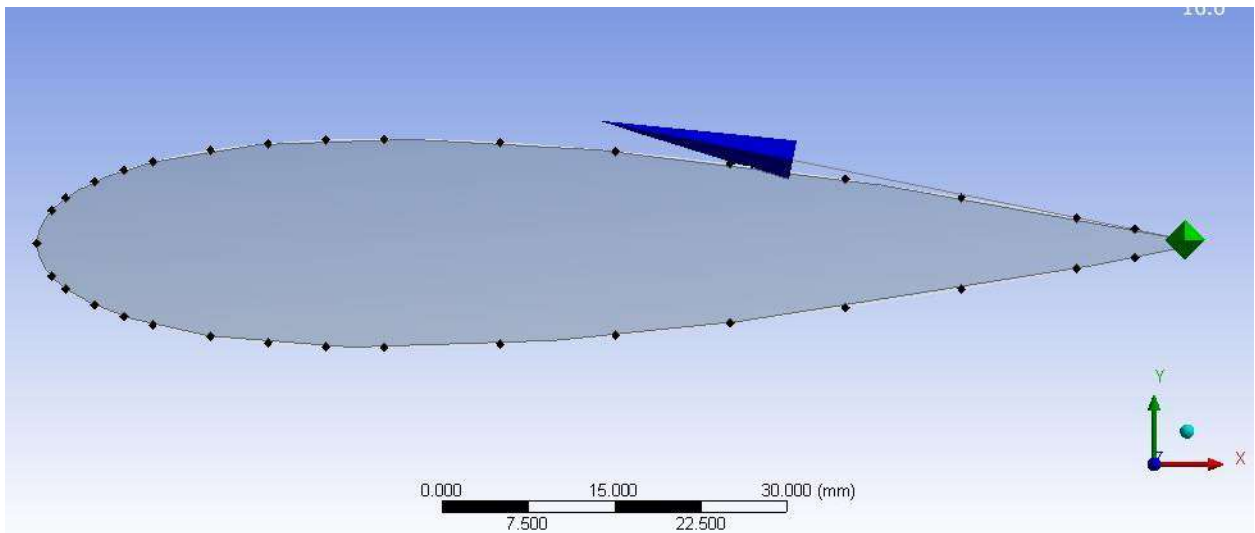
Figure 31 NACA 0018 in the 2D plane

Then extrude command was used to increase the blade size up to the requirement in the analysis.

Then to import the data on the Ansys software and to start procedure open the geometry and import the data there and generate and profile will be shown.

3. **Meshing**

Meshing is a process to divide a body in small equal pieces and it is done because by dividing in equal pieces all the force and other factors can be easily observed on these small size pieces. Meshing has many types but mostly used types are triangular and hex-dominant mesh, and we used hex-dominant mesh. Then the next step was the meshing of the NACA-0018 and meshing was done in triangle while the mesh size was 5mm.

4. **Setup and Boundary Conditions**

After meshing the next step was setup. In setup we specify the sides as velocity inlet, pressure outlet and remaining sides will be considered as the walls. And apply the boundary condition as required.

5. **Lift Co-efficient**

In next step, by applying the boundary conditions lift co-efficient were extracted.

6. **Velocity and Pressure Distribution Graphs**

Final step was the extraction of results and the velocity and pressure distribution graphs are;

Chapter 5 Result and discussion

5.1 Experimental and theoretical Results

For theoretical calculations

As we know that

$$P = \frac{1}{2}\rho A V^3 C_p$$

A= Swept Area $= H \times D = 0.8 \times 0.5 = 0.4 m^2$

$\rho = Density = 1.225 \; kg/m^3$

V= wind velocity = 3.88m/s

$C_p = 0.3$

$$P = 4.293W$$

For experimental output power

As we know that

$$P = VI$$

Where 'V' is the voltage and 'I' is the current.

Applying the very same wind speed in the wind tunnel, we used DMM to calculate the value of the voltage and current.

I = 0.23A

V = 9V

Then, $\hspace{4cm}$ P = 9×0.23

$$P = 2.07W$$

We know from experiments that power fluctuates as wind speed changes. Power likewise lowers with changeable relation as we lower the value of air. By adding load, current values in a series connection were calculated.

After the experiment, we discovered that the calculated results of the experiment and our theory disagree. The vertical axis wind turbine's massive structure and vibration are to blame for these inaccuracies. These mistakes could be the result of human error. Tip loss is another consequence that reduces lift force and increases drag force close to an airfoil's extremities as

the high-pressure air upon that lower foil surface "spills over" to the upper surface's limited pressure zone. This mistake may also be brought on by the resistance between gears, the use of improperly greased bearings, or the fact that the wind tunnel air is not properly striking the wind turbine blades.

5.2 CFD Results

Table 5-1 CFD results

Angle of attack	Lift Coefficient
0°	0.016005
2°	0.15018
4°	0.3097
6°	0.4677
8°	0.6247
10°	0.7472
12°	0.8518
14°	0.8361
16°	0.7219

Direction of angles of attack
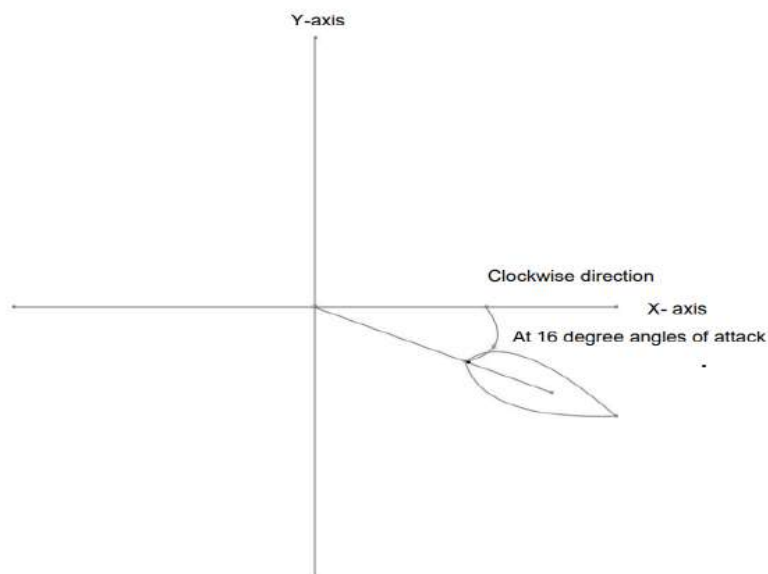
Figure 32 Shows the direction of angle of attack

The figures 32 and 33 below show the pressure and velocity patterns in relation to the airfoil caused by the airflow. It is clear that the pressure is greater at the airfoil's leading edge and as such the velocity at the airfoil's upper portion is the same as the velocity at the airfoil's lower section. According to this, the airfoil's lift and drag output at a 0 ° angle of attack is negligibly small and extremely close to zero.
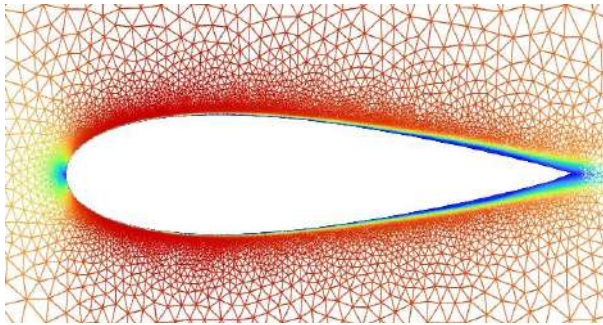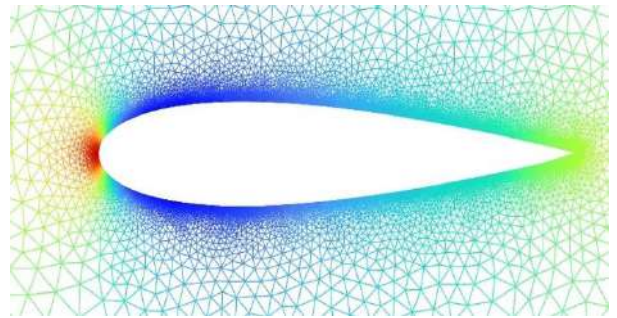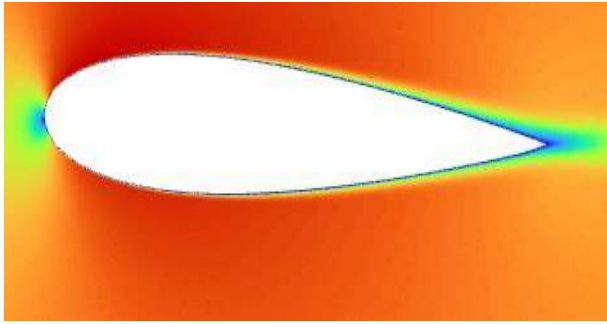

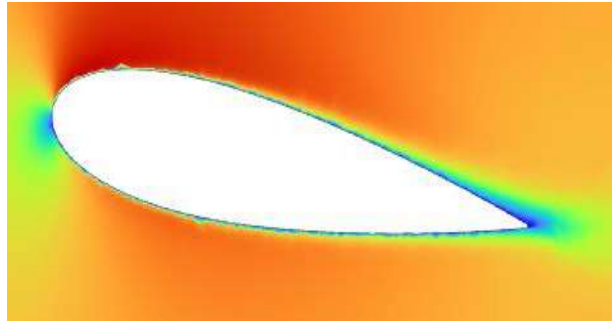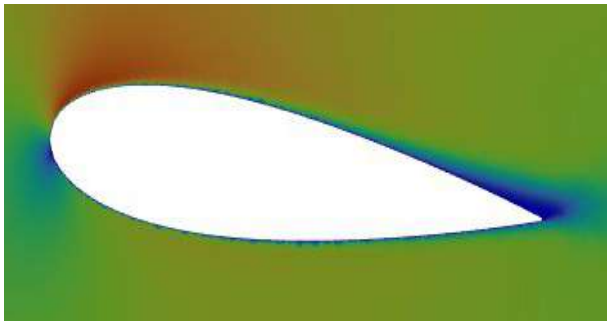Figure 33 Velocity contour at 0-degree angle of attack
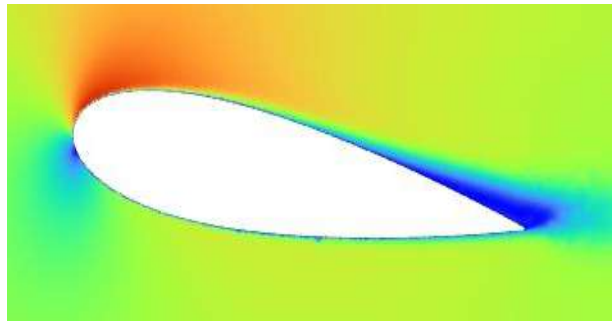

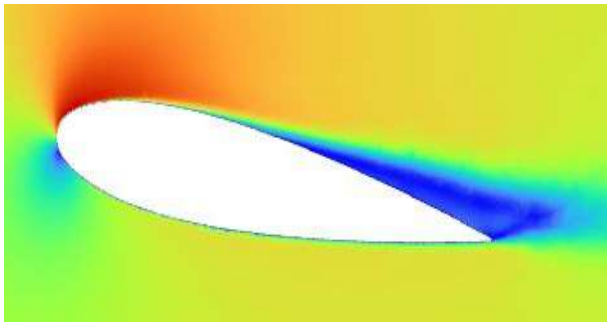Figure 34 Pressure contour at 0-degree angle of attack
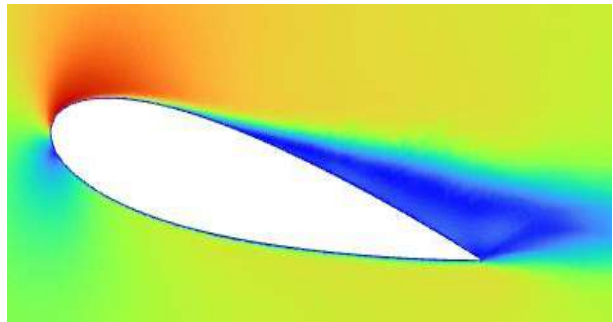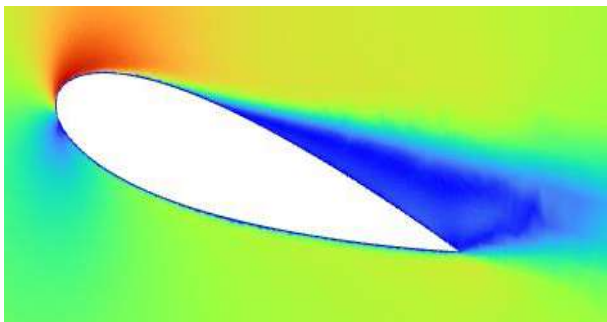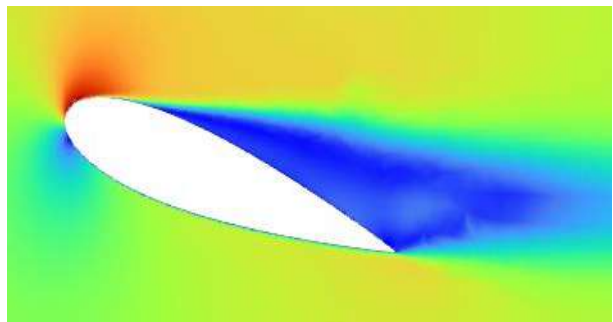
(a)

(b)

(c)

(d)

(e)

(f)

(g)

(h)

(e) Figure 35 Velocity contour at various angles of attack (a) 2° (b) 4° (c) 6° (d) 8° (e) 10°

(f) 12° (g) 14° (h) 16°

By analyzing the velocity contour in Figure 35, It is evident that all of the blades' leading edges have lower velocities, which supported the presence of stagnation points (a place where the airflow splits to flow on either side of a body in the airstream near the leading edge or nose). On the other side, as can be seen from the uneven wind velocities all along blade, the velocity contour in Figure 34 also supported whether flow separation had transpired along the blade. The huge green spot in Figure 35 shows how this phenomenon has created a notable increase in velocity in the wake zone.

The fluctuation of lift coefficient with angle of attack is seen in Table 5-2. The lift coefficient rises consistently for angles of attack between 2° and 12°, as shown in Table 5-3. Up to the maximum value observed at 12°, the lift coefficient increases with every increase in angle of attack. Beyond this angle, the lift coefficient gradually decreases. The airfoil's stalling angle is known as this angle.

Comparison between research paper and experimental CFD values

Table 5-2 Lift coefficient

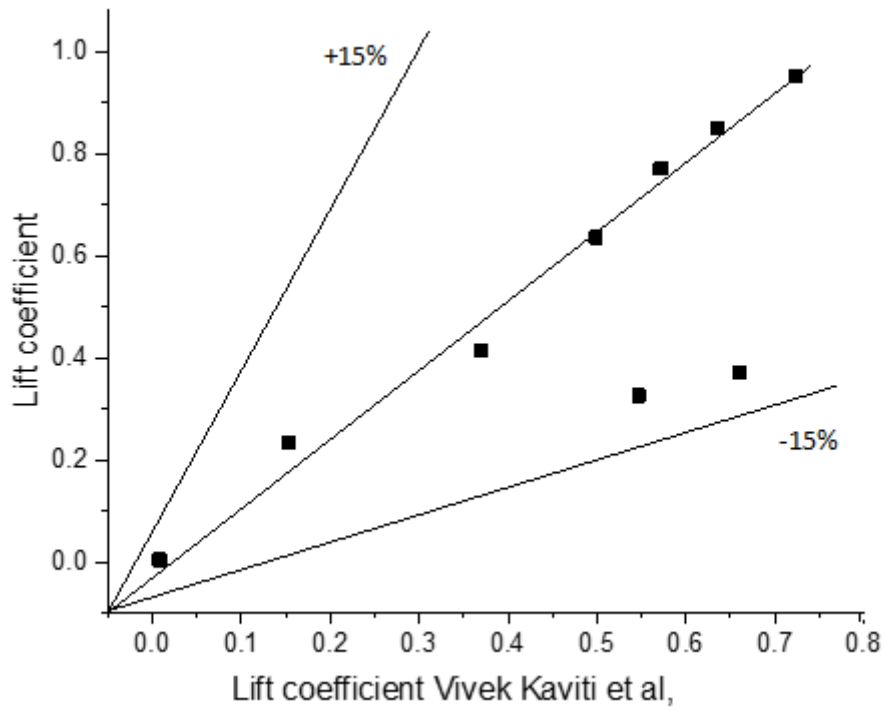| Lift Coefficient (Literature)	Lift Coefficient (Current study)	Difference (%)
0.00804598	0.016005	0.80%
0.152874	0.15018	-0.27%
0.370115	0.3097	-6.04%
0.498851	0.4677	-3.12%
0.571264	0.6247	5.34%
0.635632	0.7472	11.16%
0.724138	0.8518	12.77%
0.65977	0.8361	17.63%
0.547126	0.7219	17.48%

Validation

Figure 35 Parity plot of CFD study against Literature

We have verified our findings with the work of Vivek Kaviti et al., and we have created a parity plot to demonstrate this verification.

Chapter 6 Conclusion and future work

6.1 Conclusion

Finding renewable resources is vital as growth progresses. The use of fossil fuels to meet energy needs is getting harder and harder as time goes on. In addition to harming our ecosystem and disturbing life in many ways, utilizing fossil fuels doesn't really appear to be a sustainable option to the world's ever growing energy needs. The fastest-growing renewable energy source on land worldwide is wind power. The government is committed to providing this energy at a reasonable cost, and there is a lot more research and development being done in this area of the economy. Worldwide, wind power tends to increase at a rate of 20% to 30% annually. The cost of wind energy has decreased over time as a result of this rapid expansion, bringing the prices down to a level that is competitive. In the previous 20 years, Pakistan's energy usage has tripled. The improvements needed to meet the necessary demands are still far behind the rising energy demands. Natural gas, hydropower, nuclear energy, and oil are Pakistan's main sources of energy. Oil is used to produce 45% of the energy that is supplied for commercial purposes. 34% of the overall commercial energy supply is made up of natural gas, while roughly 15% comes from hydropower. Due to the finite supply of fossil fuels, there is a greater need for wind energy, which can be supplied by wind turbines to close the energy gap.

We examine the lift coefficient of the NACA 0018 profile at various angles of attack and come to a conclusion that the lift coefficient values increase with an increase in the angle of attack. The stalling point is when the lift coefficient reaches its greatest, which is 0.8518 at a 12-degree angle of attack. After 12-degree angles of attack, the lift coefficient rapidly declines to 0.8361 at 14 degrees and 0.7219 at 16-degree angles of attack. We came to the conclusion that a wind turbine can only hold up a maximum of 59% of the wind's energy after researching Betz's Law. We used SolidWorks and CAD software to develop our product in order to gain a sense of the actual prototype while developing, and the project's viability was assessed at each stage.

The blades, frames, and airfoil were built with careful design, which aided in the creation of the prototype. In a word, the developing and making of a vertical axis wind turbine gave us the chance to systematically apply our understanding of literature to our practical work.

6.2 Recommendations for future work

- This project is in a phase where it can generate power and also can be modified to increase its efficiency.

- Anyone who wants to work on it, can do 3D analysis on CFD for the betterment of efficiency.

- Blades design can also be changed for example adding a simple dimple, a curve, or creating a flap on the surface of the blades.

- Fiber material can also be used for the betterment of efficiency because fiber is a low-weight material.

- A special type of low rpm DC motor can be used which can generate maximum output power without any fluctuation.

- Helical gears may also be used instead of spur gears to overcome losses.

References

[1]   N. weather Service, "National Weather Services," 2019. https://www.weather.gov/

[2]   OpenEI, "Wind Energy." https://openei.org/wiki/Wind_energy

[3]   J. I. Tsutsumi, T. Katayama, T. Hayashi, H. Kitayama, and A. Ishii, "Statistical analysis for the characteristics of sea-land breeze and its effect on urban thermal environment," *Energy Build.*, vol. 16, no. 3–4, pp. 1003–1008, 1991, doi: 10.1016/0378-7788(91)90095-K.

[4]   "Science Direct." https://www.sciencedirect.com/topics/engineering/land-breeze

[5]   "WINDPOWER.org." http://ele.aut.ac.ir/~wind/en/tour/index.htm

[6]   "WW2010.atmos." http://ww2010.atmos.uiuc.edu/(Gh)/guides/mtr/home.rxml

[7]   "Danish wind industry association." http://www.windpower.org/en

[8]   J.W.Telford, *Build your own wind trubine*.

[9]   "Linquip Technews." https://www.linquip.com/blog/types-of-wind-turbines/

[10]   V. Shukla and A. K. Kaviti, "Performance evaluation of profile modifications on straight-bladed vertical axis wind turbine by energy and Spalart Allmaras models," *Energy*, 2017, doi: 10.1016/j.energy.2017.03.071.

[11]   O. S. Gim and G. W. Lee, "Flow characteristics and tip vortex formation around a NACA 0018 foil with anendplate," *Ocean Eng.*, vol. 60, pp. 28–38, Mar. 2013, doi: 10.1016/J.OCEANENG.2012.12.009.

[12]   S. Brusca, • R Lanzafame, and • M Messina, "Design of a vertical-axis wind turbine: how the aspect ratio affects the turbine's performance," *Int J Energy Env. Eng*, vol. 5, pp. 333–340, 2014, doi: 10.1007/s40095-014-0129-x.

[13]   "IOP Conference Series: Earth and Environmental Science", doi: 10.1088/1755-1315/573/1/012047.

[14]   J. O. Dabiri, "Potential order-of-magnitude enhancement of wind farm power density via counter-rotating vertical-axis wind turbine arrays," *J. Renew. Sustain. Energy*, vol. 3, no. 4, 2011, doi: 10.1063/1.3608170.

[15]   R. G. J. Flay *et al.*, "Journal of Wind Engineering & Industrial Aerodynamics Wind speed measurements and predictions over Belmont Hill , Wellington , New Zealand," *J. Wind Eng. Ind. Aerodyn.*, vol. 195, no. January, p. 104018, 2019, doi: 10.1016/j.jweia.2019.104018.

[16]   M. Moshfeghi and N. Hur, "Journal of Wind Engineering & Industrial Aerodynamics Power generation enhancement in a horizontal axis wind turbine blade using split blades," *J. Wind Eng. Ind. Aerodyn.*, vol. 206, no. September, p. 104352, 2020, doi: 10.1016/j.jweia.2020.104352.

[17]   R. D. Ionescu, I. Szava, S. Vlase, M. Ivanoiu, and R. Munteanu, "Innovative Solution of Vertical Axis Wind Turbine, Suitable for Naval Industry Implementation (Numerical Methods and Analythical Calculus)," *Procedia Technol.*, vol. 19, pp. 715–721, Jan. 2015, doi: 10.1016/J.PROTCY.2015.02.101.

[18] R. Corniglion, J. C. Harris, and C. Peyrard, "The aerodynamics of a blade pitch, rotor speed, and surge step for a wind turbine regarding dynamic inflow," *Wind Energy*, vol. 25, no. 5, pp. 858–880, 2022, doi: 10.1002/we.2702.

[19] D. B. Araya, "Aerodynamics of vertical-axis wind turbines in full-scale and laboratory-scale experiments," *Caltech PhD Thesis*, vol. 2016, 2016.

[20] M. Anthony, V. Prasad, K. Raju, M. H. Alsharif, Z. W. Geem, and J. Hong, "Design of rotor blades for vertical axis wind turbine with wind flow modifier for low wind profile areas," *Sustain.*, vol. 12, no. 19, pp. 1–24, 2020, doi: 10.3390/su12198050.

[21] P. L. Delafin, T. Nishino, L. Wang, and A. Kolios, "Effect of the number of blades and solidity on the performance of a vertical axis wind turbine," *J. Phys. Conf. Ser.*, vol. 753, no. 2, 2016, doi: 10.1088/1742-6596/753/2/022033.

[22] G. Diwakar, N. V. S. S. L. Narayana, Y. Raviram, B. S. Sujan, and S. B. Prakash, "Design and analysis of vertical axis wind turbine blade," *Int. J. Mech. Eng. Technol.*, vol. 8, no. 5, pp. 504–509, 2017.

[23] A. Shires and V. Kourkoulis, "Application of circulation controlled blades for vertical axis wind turbines," *Energies*, vol. 6, no. 8, pp. 3744–3763, 2013, doi: 10.3390/en6083744.

[24] A. Siddiqui, A. Hameed, S. N. Mian, and R. Khatoon, "255 . Experimental Investigations of Hybrid Vertical Axis Wind Turbine," *4th Int. Conf. Energy, Environ. Sustain. Dev. 2016 (EESD 2016)*, vol. 2016, no. Eesd, 2016.

[25] M. Balaji, K. A. Satheesh, G. Sanjay, and H. K. Job, "DESIGN OF THROTTLE BODY : A COMPARATIVE STUDY OF DIFFERENT SHAFT PROFILES USING CFD ANALYSIS," vol. 14, pp. 681–686, 2016.

[26] M. Richmond, A. Antoniadis, L. Wang, A. Kolios, S. Al-Sanad, and J. Parol, "Evaluation of an offshore wind farm computational fluid dynamics model against operational site data," *Ocean Eng.*, vol. 193, no. October, p. 106579, 2019, doi: 10.1016/j.oceaneng.2019.106579.

[27] L. Wang, R. Quant, and A. Kolios, "Fluid structure interaction modelling of horizontal-axis wind turbine blades based on CFD and FEA," *J. Wind Eng. Ind. Aerodyn.*, vol. 158, pp. 11–25, 2016, doi: 10.1016/j.jweia.2016.09.006.

[28] M. M. Elsakka, D. B. Ingham, L. Ma, and M. Pourkashanian, "CFD analysis of the angle of attack for a vertical axis wind turbine blade," *Energy Convers. Manag.*, vol. 182, no. January, pp. 154–165, 2019, doi: 10.1016/j.enconman.2018.12.054.

[29] M. Hassanpour and L. N. Azadani, "Aerodynamic optimization of the configuration of a pair of vertical axis wind turbines," *Energy Convers. Manag.*, vol. 238, p. 114069, 2021, doi: 10.1016/j.enconman.2021.114069.

[30] L. R. Amjith and B. Bavanish, "Design and analysis of 5 MW horizontal axis wind turbine," *Mater. Today Proc.*, vol. 37, no. Part 2, pp. 3338–3342, 2020, doi: 10.1016/j.matpr.2020.09.202.

[31] P. Negi and M. Subhash, "Method to control flow separation over wind turbine blade: A CFD study," *Mater. Today Proc.*, vol. 46, no. xxxx, pp. 10960–10963, 2021, doi: 10.1016/j.matpr.2021.02.040.

[32] S. K. Thangavelu, S. F. Chow, C. C. V. Sia, and K. H. Chong, "Aeroelastic performance analysis of horizontal axis wind turbine (HAWT) swept blades," *Mater. Today Proc.*, vol. 47, no. xxxx, pp. 4965–4972, 2021, doi: 10.1016/j.matpr.2021.04.315.

[33] S. Sahebzadeh, A. Rezaeiha, and H. Montazeri, "Towards optimal layout design of vertical-axis wind-turbine farms: Double rotor arrangements," *Energy Convers. Manag.*, vol. 226, no. November, p. 113527, 2020, doi: 10.1016/j.enconman.2020.113527.

[34] I. C. M. Lositaño and L. A. M. Danao, "Steady wind performance of a 5 kW three-bladed H-rotor Darrieus Vertical Axis Wind Turbine (VAWT) with cambered tubercle leading edge (TLE) blades," *Energy*, vol. 175, pp. 278–291, 2019, doi: 10.1016/j.energy.2019.03.033.

[35] M. H. Mohamed, A. Dessoky, and F. Alqurashi, "Blade shape effect on the behavior of the H-rotor Darrieus wind turbine: Performance investigation and force analysis," *Energy*, vol. 179, pp. 1217–1234, 2019, doi: 10.1016/j.energy.2019.05.069.

[36] J. Chen, X. Pan, C. Wang, G. Hu, H. Xu, and P. Liu, "Airfoil parameterization evaluation based on a modified PARASEC method for a H-Darrious rotor," *Energy*, vol. 187, p. 115910, 2019, doi: 10.1016/j.energy.2019.115910.

[37] A. Posa, "Influence of Tip Speed Ratio on wake features of a Vertical Axis Wind Turbine," *J. Wind Eng. Ind. Aerodyn.*, vol. 197, no. December 2019, p. 104076, 2020, doi: 10.1016/j.jweia.2019.104076.

[38] H. Day, D. Ingham, L. Ma, and M. Pourkashanian, "Adjoint based optimisation for efficient VAWT blade aerodynamics using CFD," *J. Wind Eng. Ind. Aerodyn.*, vol. 208, no. April, p. 104431, 2021, doi: 10.1016/j.jweia.2020.104431.

[39] M. Kumar Rathore, M. Agrawal, and P. Baredar, "Energy production potential from the wake of moving traffic vehicles on a highway by the array of low economic VAWT," *Mater. Today Proc.*, vol. 46, no. xxxx, pp. 5272–5277, 2020, doi: 10.1016/j.matpr.2020.08.638.

[40] "Design & construction of a Vertical Axis Wind Turbine", [Online]. Available: https://ieeexplore.ieee.org/document/6991132

[41] Wikipedia, "NACA airfoil," 2022.